



## Synthesis and evaluation of PEGylated amino pyrimidines coated on gold and silver nanoparticles as drug delivery system for anticancer activity

Nitin K. Longadge<sup>1\*</sup> and Anjali M. Rahatgaonkar<sup>2</sup>

<sup>1</sup>Department of Chemistry, Institute of Science, Nagpur, Maharashtra, India

<sup>2</sup>Department of Forensic Chemistry and Toxicology, Institute of Forensic Science, Nagpur, Maharashtra, India

### ABSTRACT

A series of PEGylated amino pyrimidines surfaced on to gold and silver nanoparticles was designed, synthesized and evaluated for anticancer activity against three human cancer cell lines: U2OS osteosarcoma, MB231 breast cancer and SW480 colon carcinoma. Non-PEGylated and nanoparticles linked PEGylated pyrimidines exhibited moderate to potent activity against U2OS and MB231. Among them, the PEGylated amino pyrimidines showed excellent broad spectrum activity with  $IC_{50}$  values ranging from 13 to 346  $\mu$ M. Particularly, the PEGylated amino pyrimidines with thiophene ring at C2 showed significant potency against all tested human cancer cell lines. The morphology of all the compounds was tested by TEM and XRD. In this study, two independent approaches that conjugating pyrimidines to PEG<sub>(200)</sub> and mounting this passive targeting moieties onto the NPs were adopted to fabricate pyrimidine-PEG-AuNPs and pyrimidine-PEG-AgNPs. The NPs synthesized in this study were proven able to effectively target PEGylation to cancer cells, and showed profound apoptotic induction effect to those cells. Although the drug efficacy was compromised after conjugation with Au and Ag, the resultant could still make this moiety NPs a good candidate for anticancer therapy.

**Keywords:** PEG, Nanoparticles, Pyrimidines, anticancer activity, antioxidant activity

### INTRODUCTION

Cancer, medically termed as malignant neoplasm, is a class of serious diseases that the proliferating mammalian cells present unlimited abnormal growth behaviors, invasion to adjacent tissues by intrusion and destruction of surrounding matrix, migration from the original location to other near end sites and finally metastasis through blood and lymph node vessels to distant organs[1].

Extensive research on diverse biological activities of aza-heterocycles has confirmed their immense significance in pathophysiology of diseases. The amalgamation of two pharmacologically important structural scaffolds leads to a new library of heterocycles, possessing broad spectrum of activities against numerous pathogenic strains and also striking activities against cancer[2]. Pyrimidines play an important role in drug discovery process and have considerable pharmacological and chemical importance. Recently, thienopyrimidine derivatives have been evaluated for their broad bioactivities, including antitumor [3], anti-microbial [4], anti-inflammatory[5], anti-leukemic [6], anti-filarial[7]activities (Figure 1).

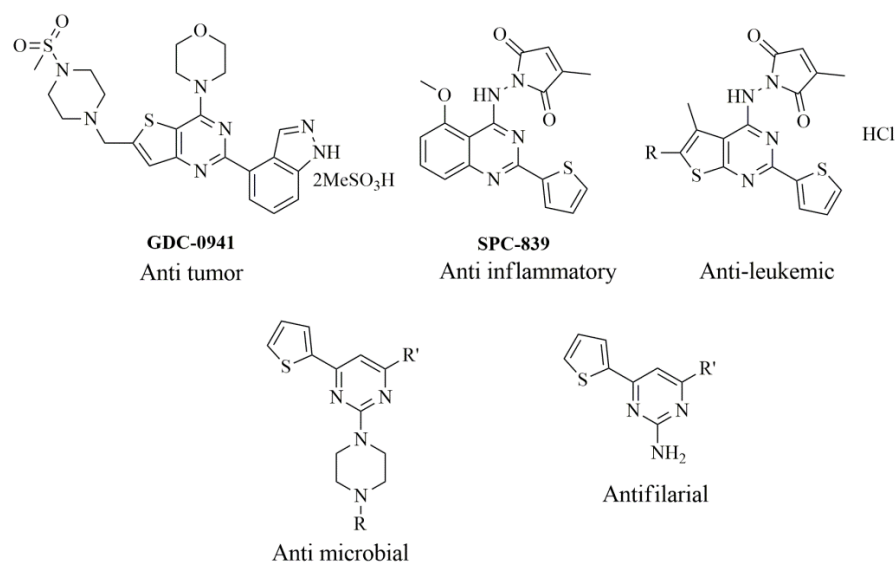


**Fig. 1** Example of pharmacologically important thieophene pyrimidine

The combination of different treatments in cancer therapy has drawn massive attention in the last decades due to its superior anticancer ability to single treatment. One of the most useful strategies to achieve this purpose is to design and construct efficient multifunctional nano-platforms[8].

Nanomaterials are typically conjugated to a targeting moiety, thereby permitting preferential accumulation of the drug within specific tissues, individual cancer cells, or to be associated with specific molecules within cancer cells[9].

Meanwhile, the nano-particulate delivery system is believed to increase the stability of the encapsulated or conjugated therapeutical molecules, improve the efficacy, and alleviate the undesired side-effects [10-11]. Active targeting is programmed by engineering nanoparticle with cellular specific targeting moieties, whilst it is difficult to realize without passive targeting, in which poly(ethylene glycol) (PEG) is normally chosen to attenuate the surrounding environment (commonly aqueous or body fluid) to the nanoparticles to protect them from protein absorption and also to prolong the circulation time after administration into the body [12]. Polyethylene glycol (PEG) has been widely utilized in recent cancer research due to its water solubility and bio-compatibility. PEG can be functionalized via the hydroxyl groups[13-14].

We have synthesized various building blocks, scaffolds, and high value intermediates by selective functionalization, generation and derivatization of privileged structures. We have generated important pathways for synthons deemed promising for the syntheses of other important derivatives of pyrimidines. Introduction of substituents like nitro, thiophene and furan moiety is facile. A library of nine PEGylated pyrimidine derivatives surfaced on NPs was evaluated as anticancer agents against human cancer cell lines: U2OS osteosarcoma, MB231 breast cancer and SW480 colon carcinoma. The observations suggested that they could constitute a unique class of inhibitors. Diversity of substitution at various points on the skeleton of PEGylated pyrimidine derivatives leads to significantly modulated selectivity in the active site cavity. The spectroscopic analysis and transmission electron microscopic (TEM) analysis played a pivotal role in characterization.

## EXPERIMENTAL SECTION

### Chemistry

#### Materials and Instrumentations

Chloroauric acid ( $\text{HAuCl}_4 \cdot 4\text{H}_2\text{O}$ ) was obtained from Acros Organics (New Jersey, USA), Silver nitrate ( $\text{AgNO}_3$ ),  $\text{NaBH}_4$ , trisodium citrate were procured from Sigma- Aldrich (St. Louis, MO, USA), PEG<sub>200</sub> was obtained from SD-Fine chemicals Ltd. (Mumbai, India), all other reagents required for the synthesis of the nanoparticles conjugated PEGylated pyrimidines were of synthesis grade and purchased from Acros Organics, Sigma-Aldrich, Qualigens and SD-Fine Chemicals. All solvents were distilled prior to use. Water purified by a Millipore system was used for making the solutions. Thin-layer chromatography was performed on silica gel G. Melting points were determined by the open capillary method and are uncorrected. Human osteosarcoma cell line, U2OS (ATCC Catalog No. HTB-96, USA) was cultured in RPMI 1640 culture medium supplemented with L-Glutamine, human breast cancer cell

MB231 (ATCC Catalog No. HTB-26, USA) were grown in DMEM medium, and colon carcinoma cell line, SW480 (ATCC Catalog No. CCL-228), the base medium for cell lines was ATCC-formulated Leibovitz's L-15 Medium, Catalog No. 30-2008. Alamar blue sodium salt, saline phosphate buffer and 0.25% trypsin-EDTA solution were procured from Sigma-Aldrich.

Absorption measurements were carried out on Shimadzu UV-1700 Pharma Spec. The FT-IR measurements for samples were carried out using KBr pallets on Shimadzu FT-IR spectrophotometer. The  $^1\text{H}$  NMR spectra and  $^{13}\text{C}$  NMR spectra were recorded in  $\text{DMSO}-d_6/\text{CDCl}_3$  on a Bruker Avance II 400 NMR spectrometer. Chemical shifts are reported using TMS as an internal standard. Mass spectra were recorded using a Shimadzu gas chromatograph. Elemental analyses were performed on a Perkin Elmer 2400 instrument. Samples for transmission electron microscope (TEM) were prepared by putting a drop of the colloidal solution on a copper grid coated with a thin amorphous carbon film. Samples were dried and kept under vacuum in desiccators before putting them in a specimen holder. TEM characterization was carried out using a Philips CM-200 electron microscope. Particle size was measured from the TEM micrographs. The particle size was calculated by taking average of at least 100 particles. The X-ray diffraction patterns have been recorded in  $2\theta$  range from  $20$  to  $80^\circ$  on Philips (Holland) automated X-ray powder diffractometer. The operating target voltage was 35kV and tube current was 20mA. The scanning speed was  $0.5$   $2\theta/\text{min}$ . Radiation used was Cu-k of wavelength  $1.54056 \text{ \AA}$  provided with a monochromator for filtering  $\beta$  radiations to reduce noise due to white radiations and to increase the resolution. The values of inter-planer spacing ( $d$ ) corresponding to Bragg reflections ( $2\theta$ ) were obtained. Indexing and calculations of unit cell parameters were performed with the help of Powder-X-Software[15-17].

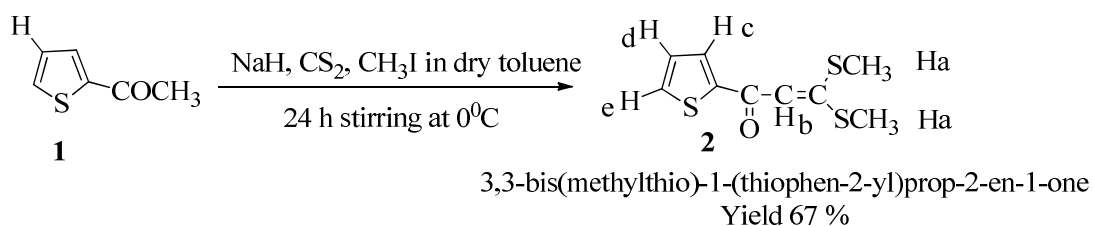
#### Synthesis of 1-(4-nitrothiophen-2-yl)ethanone(1a)

In a 125mL conical flask, 1.5mL 2-acetyl thiophene **1** ( $R_f = 0.74$ ) and approximately 4.0mL of concentrated sulfuric acid (drop-wise) was added, the reaction mixture was continued to cool in the ice bath. After complete addition of sulfuric acid, approximately 2.0 mL concentrated nitric acid was added drop-wise. The reaction mixture was kept at room temperature for fifteen minutes; it was poured in 100mL of ice cold water. The product was isolated by vacuum filtration, washed with ice cold water (20 mL). The crude material **1a** was purified by recrystallization from a small volume ( $\sim 10$  mL) of hot methanol ( $R_f = 0.95$ ). Light brown solid, yield 52 %; m.p.:  $126^\circ\text{C}$ ; IR (KBr)  $\lambda_{\text{max}}/\text{cm}^{-1}$ : 2915 ( $-\text{CH}_3$ ), 1680 ( $-\text{C}=\text{O}$ ), 1520 ( $-\text{NO}_2$ );  $^1\text{H}$  NMR (400 MHz,  $\text{CDCl}_3/\text{DMSO}-d_6$ ,  $\square$ , ppm):  $\delta$  2.5 (s, 3H,  $-\text{CH}_3$ ), 8.13 (s, 1H, Thiophene- $\text{H}_c$ ), 8.54 (s, 1H, Thiophene- $\text{H}_e$ );  $^{13}\text{C}$  NMR (100 MHz,  $\text{CDCl}_3/\text{DMSO}-d_6$ , ppm):  $\delta$  26.8, 125.1, 132.7, 145.0, 148.1, 190.6; GCMS (m/z): 171 ( $\text{M}^+$ ); Anal. calcd. for  $\text{C}_6\text{H}_5\text{NO}_3\text{S}$ : C: 42.10, H: 2.94, N: 8.18; Found: C: 42.06, H: 2.90, N: 8.16.

#### Synthesis of 3,3-bis(methylthio)-1-(thiophen-2-yl)prop-2-en-1-one (2)

An ice chilled solution of 2-acetyl thiophene **1** (3 mL, 28 mmol) in dry toluene (50 mL) was treated with NaH (2.3 g, 2 mmol) and the mixture was stirred at  $0^\circ\text{C}$  for 10 min., carbon disulphide (2.52 mL, 1.5 mmol) and methyl iodide (5.23 mL, 3 mmol) were added to the cold solution drop wise over a period of 20 min. The mixture was kept below  $10^\circ\text{C}$ . After the mixture was stirred for 24 h at room temperature ( $R_f = 0.75$ ), a small amount of crash ice was added. The toluene was removed at reduced pressure and the residue was portioned between water and chloroform. The organic layer was dried ( $\text{Na}_2\text{SO}_4$ ) and evaporated at reduced pressure. The residue was recrystallized from absolute alcohol to furnish 3,3-bis(methylthio)-1-(thiophen-2-yl)prop-2-en-1-one as yellow needles ( $R_f = 0.60$ ) displayed in Scheme 1.

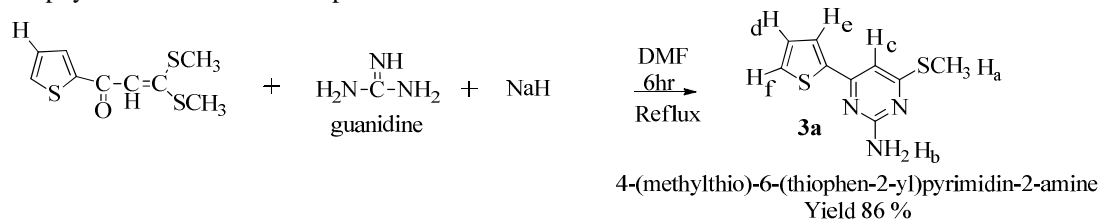
Yellow needles solid, yield 67 %; m.p.:  $110^\circ\text{C}$ ; IR (KBr)  $\lambda_{\text{max}}/\text{cm}^{-1}$ : 3104 ( $\text{CH}=\text{C}$ ), 2988, 2916 ( $-\text{S}-\text{CH}_3$ ), 1745 ( $-\text{C}=\text{O}$ ), 1071 ( $\text{C}-\text{S}$ );  $^1\text{H}$  NMR (400 MHz,  $\text{CDCl}_3/\text{DMSO}-d_6$ ,  $\delta$ , ppm):  $\delta$  2.51 (s, 3H,  $-\text{SCH}_3$ ), 2.61 (s, 3H,  $-\text{SCH}_3$ ), 6.67 (s, 1H,  $-\text{CH}-$ ), 7.13-7.14 (t, 1H,  $J=3.8$ , Thiophene- $\text{H}_d$ ), 7.63-7.64 (d, 1H,  $J=4$ , Thiophene- $\text{H}_c$ ), 7.72-7.80 (d, 1H,  $J=4.12$ , Thiophene- $\text{H}_e$ );  $^{13}\text{C}$  NMR (100 MHz,  $\text{CDCl}_3/\text{DMSO}-d_6$ , ppm):  $\delta$  17.65, 108.05, 129.0, 130.15, 132.64, 139.57, 165.68, 180.45; GCMS (m/z): 229 ( $\text{M}^+$ ); Anal. calcd. for  $\text{C}_9\text{H}_{10}\text{OS}_3$ : C: 46.92, H: 4.38, S: 41.76; Found: C: 46.86, H: 4.32, S: 41.70.



Scheme 1 Synthesis of 3,3-bis(methylthio)-1-(thiophen-2-yl)prop-2-en-1-one 2

**Synthesis of 4-(methylthio)-6-(thiophen-2-yl)pyrimidin-2-amine (3a)**

3,3-bis(methylthio)-1-(thiophen-2-yl)prop-2-en-1-one (2 mmol) was dissolved in DMF (20 mL) at room temperature then guanidine carbonate (0.192 g, 2 mmol) and NaH (0.55 g, 4 mmol) were added. The solution ( $R_f=0.88$ ) was refluxed for 6 h. The mixture was cooled and poured into ice cold water (50 mL). The solid obtained was filtered off, dried, and purified using column chromatography on silica gel (60x120) with ethyl acetate–hexane (3:7) mixture as eluent. The product (Scheme 2) ( $R_f=0.61$ ) was obtained as off-white solid, yield 86 %; m.p.: 180°C; IR (KBr)  $\lambda_{max}/cm^{-1}$ : 3400, 3325 (-NH<sub>2</sub>), 2915 (-CH<sub>3</sub>), 1610  $cm^{-1}$  (-C=C- in aromatic ring); <sup>1</sup>H NMR (400 MHz, CDCl<sub>3</sub>/DMSO-d<sub>6</sub>,  $\delta$ , ppm):  $\delta$  2.45 (s, 3H, -SCH<sub>3</sub>), 5.04 (s, 2H, -NH<sub>2</sub>), 6.76 (s, 1H, Ar-H), 7.01-7.04 (t, 1H,  $J=4.72$ , Thiophene-H<sub>d</sub>), 7.30-7.32 (d, 1H,  $J=4.8$ , Thiophene-H<sub>e</sub>), 7.560-7.569 (d, 1H,  $J=3.36$ , Thiophene-H<sub>f</sub>); <sup>13</sup>C NMR (100 MHz, CDCl<sub>3</sub>/DMSO-d<sub>6</sub>, ppm):  $\delta$  14.17, 102.93, 126.71, 128.08, 129.01, 142.56, 157.93, 162.23, 171.56; GCMS (m/z): 223 (M<sup>+</sup>); Anal. calcd. for C<sub>9</sub>H<sub>9</sub>N<sub>3</sub>S<sub>2</sub>: C: 48.40, H: 4.06, N: 18.82; Found: C: 48.42, H: 4.04, N: 18.78. The physicochemical data is depicted in Table 1.



Scheme 2 Synthesis of 4-(methylthio)-6-(thiophen-2-yl)pyrimidin-2-amine 3a

Table 1 Physical characterization data of substituted pyrimidine derivatives 3a-c

Entry	Product	Mol. Weight	Yield (%)	m.p. (°C)	Mol. Formula
3a		223	86	170	C <sub>9</sub> H <sub>9</sub> N <sub>3</sub> S <sub>2</sub>
3b		268	82	130	C <sub>9</sub> H <sub>8</sub> N <sub>4</sub> O <sub>2</sub> S <sub>2</sub>
3c		207	83	180	C <sub>9</sub> H <sub>9</sub> N <sub>3</sub> OS

**Synthesis of 4-(methylthio)-6-(4-nitrothiophen-2-yl)pyrimidin-2-amine (3b)**

3,3-bis(methylthio)-1-(4-nitrothiophen-2-yl)prop-2-en-1-one (2 mmol) was dissolved in DMF (20 mL) at room temperature then guanidine carbonate (0.192 g, 2 mmol) and NaH (0.55 g, 4 mmol) were added. The solution was refluxed for 8 h. The mixture was cooled and poured into ice cold water (50 mL) and extracted with ethyl acetate (2x25 mL) evaporated at room temperature to obtain solid which was purified using column chromatography on silica gel (60x120) with ethyl acetate–hexane (2:8) mixture as eluent. The product was obtained as Brown solid, yield 72%, m.p. 195 °C; (KBr)  $\lambda_{max}/cm^{-1}$  3410, 3320 (-NH<sub>2</sub>), 2910 (-CH<sub>3</sub>), 1600  $cm^{-1}$  (-C=C- in aromatic ring), 1520 (-NO<sub>2</sub>); <sup>1</sup>H-NMR (400 MHz, CDCl<sub>3</sub>/DMSO-d<sub>6</sub>,  $\delta$ , ppm)  $\delta$  2.64 (s, 3H, -SCH<sub>3</sub>), 4.80 (s, 2H, -NH<sub>2</sub>), 6.70 (s, 1H, Ar-H), 7.46-7.47 (d, 1H,  $J=4.48$ , Thiophene-H<sub>e</sub>), 7.53-7.54 (d, 1H,  $J=3.4$ , Thiophene-H<sub>f</sub>); <sup>13</sup>C-NMR (CDCl<sub>3</sub>/DMSO-d<sub>6</sub>)  $\delta$  107.4, 118.5, 130.7, 143.2, 148.7, 160.9, 162.9, 171.3; GCMS (m/z): 268 (M<sup>+</sup>); Anal. for C<sub>9</sub>H<sub>8</sub>N<sub>4</sub>O<sub>2</sub>S<sub>2</sub> (268) Calcd.: C, 40.29; H, 3.01; N, 20.88%. Found: C, 40.27; H, 3.05; N, 20.84%.

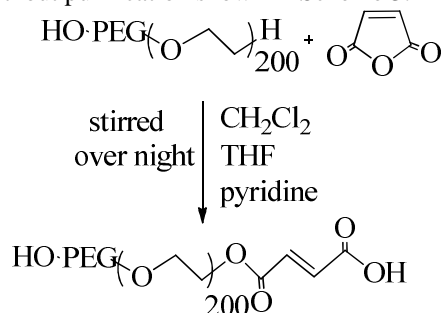
**Synthesis of 4-(furan-2-yl)-6-(methylthio)pyrimidin-2-amine (3c)**

1-(furan-2-yl)-3,3-bis(methylthio)prop-2-en-1-one (2 mmol) was dissolved in DMF (20 mL) at room temperature then guanidine carbonate (0.192 g, 2 mmol) and NaH (0.55 g, 4 mmol) were added. The solution was refluxed for 6 h. The mixture was cooled and poured into ice cold water (50 mL). The solid obtained was filtered off, recrystallized with ethanol and purified using column chromatography on silica gel (60x120) with ethyl acetate–hexane (3:7) mixture as eluent. The product was obtained as Brown solid, yield 83%, m.p. 180 °C; (KBr)  $\lambda_{max}/cm^{-1}$  3380, 3200 (-NH<sub>2</sub>), 2920 (-CH<sub>3</sub>), 1590  $cm^{-1}$  (-C=C- in aromatic ring); <sup>1</sup>H-NMR (400 MHz, CDCl<sub>3</sub>/DMSO-d<sub>6</sub>,  $\delta$ , ppm)  $\delta$  2.57 (s,

3H, -SCH<sub>3</sub>), 4.91 (s, 2H, -NH<sub>2</sub>), 6.36 (s, 1H, Ar-H), 7.08-7.11 (t, 1H, *J* = 4.72, Thiophene-H<sub>d</sub>), 7.62-7.68 (dd, 1H, *J* = 4.68, 3.16, Thiophene-H<sub>e</sub>), 7.95-7.99 (dd, 1H, *J* = 4.8, 3.12, Thiophene-H<sub>f</sub>) <sup>13</sup>C-NMR (CDCl<sub>3</sub>/DMSO-d<sub>6</sub>) δ 14.38, 107.19, 112.14, 143.02, 157.18, 162.89, 166.36, 171.22, GCMS (m/z): 207 (M<sup>+</sup>); Anal. for C<sub>9</sub>H<sub>9</sub>N<sub>3</sub>OS (207) Calcd.: C, 52.16; H, 4.38; N, 20.27%. Found: C, 52.17; H, 4.40; N, 20.25%.

### Synthesis of hydroxycarboxy poly ethylene glycol (HO-PEG<sub>200</sub>COOH)

Poly ethylene glycol (28.0mmole, 5mL) was dissolved in 20 mL of dry CH<sub>2</sub>Cl<sub>2</sub>. To this solution was added THF containing maleic anhydride (56.0mmole, 0.54mg) and pyridine (56.0mmole, 0.46mL). The mono acid derivative of poly (ethylene glycol) <sub>200</sub> was used without purification shown in Scheme 3.

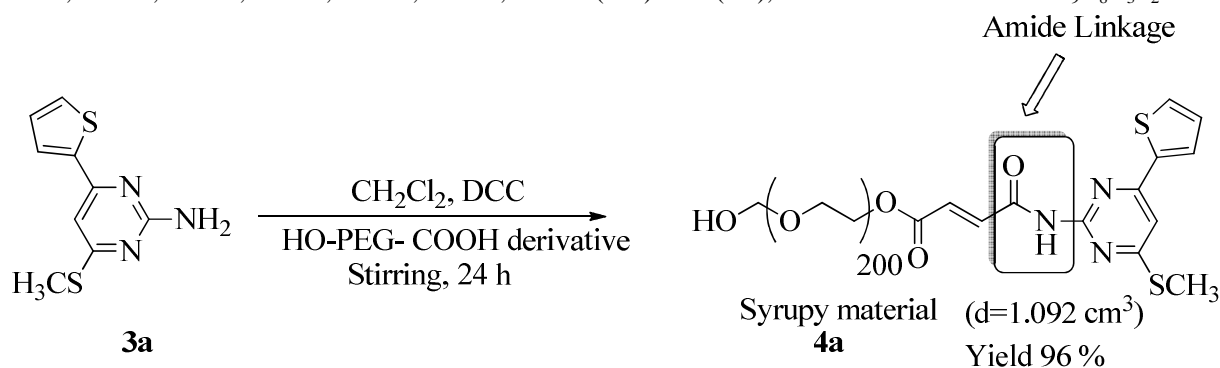


Scheme 3 Synthesis of hydroxycarboxy poly ethylene glycol (HO-PEG<sub>200</sub>COOH)

### Synthesis of N-Terminal of PEGylated-4-(methylthio)-6-(thiophen-2-yl) pyrimidin-2-amine (4a)

The mono acid derivative of carboxyhydroxy PEG (HO-PEG<sub>200</sub>COOH) (28.0mmole) was activated with 1:2 molar equivalent of 4-(methylthio)-6-(thiophen-2-yl)pyrimidin-2-amine (3a) (46.0mmole). N, N dicyclohexylcarbodiimide (46.0mmole) was dissolved in dichloromethane. (Scheme 4, Table 2) The solution was stirred for 24 h at room temperature. A syrupy resin obtained was dried under vacuum. The resin was dissolved in 15 mL of acetone. A white precipitate of dicyclohexylurea (DCU) appeared was discarded and filtrate was collected. The final filtrate was evaporated to afford the product. TLC in (methanol: ethyl acetate 7:3) was performed to check the presence of DCU. It showed a negative result. This negative result was confirmed by IR spectra. A complete amino group capping was indicated by a negative dye test.

The resin was dried in vacuum for IR, <sup>1</sup>H NMR, <sup>13</sup>C NMR and Mass characterization. At this stage the resin did not stick anymore to the glass wall. IR spectrum of resin showed the characteristic absorption band PEG ether backbone (1120 cm<sup>-1</sup>) and absorption bands 1720 and 1625 cm<sup>-1</sup> for the ester and amid bond respectively (C=O). Syrupy liquid, yield 96 %; density: 1.154cm<sup>3</sup>; IR (KBr) λ<sub>max</sub>/cm<sup>-1</sup>: 3395 (-OH, -NH), 2920 (-CH<sub>2</sub>-PEG), 2885 (-CH<sub>3</sub>), 1720 and 1625 cm<sup>-1</sup> for the ester and amid bond (-C=O, PEG); <sup>1</sup>H NMR (400 MHz, CDCl<sub>3</sub>/DMSO-d<sub>6</sub>, δ, ppm): δ 2.52 (s, 3H, -SCH<sub>3</sub>), 3.22-4.55 (m, multiple-H-PEG), 5.67 (s, 1H, -NH), 6.78 (s, 1H, Ar-H), 7.12-7.13 (t, 1H, *J* = 4.28, Thiophene-H), 7.22-7.56 (dd, 1H, *J* = 5.28, 3.2, Thiophene-H), 7.70-7.73 (dd, 1H, *J* = 4.96, 3.52 Thiophene-H); <sup>13</sup>C NMR (100 MHz, CDCl<sub>3</sub>/DMSO-d<sub>6</sub>, δppm): δ 12.56, 61.38, 64.38, 68.79, 70.44, 113.30, 127.39, 128.26, 129.32, 141.33, 146.76, 161.65, 164.86, 165.23, 169.29; GCMS (m/z): 503 (M<sup>+</sup>), Molecular formula: PEG-C<sub>9</sub>H<sub>8</sub>N<sub>3</sub>S<sub>2</sub>.



Scheme 4 Synthesis of N-Terminal of PEGylated-4-(methylthio)-6-(thiophen-2-yl) pyrimidin-2-amine 4a

### Synthesis of PEGylated-4-(methylthio)-6-(4-nitrothiophen-2-yl)pyrimidin-2-amine (4b)

The mono acid derivative of carboxyhydroxy PEG (HO-PEG<sub>200</sub>COOH) (28.0mmole) was activated with 1:2 molar equivalent of 4-(methylthio)-6-(4-nitrothiophen-2-yl)pyrimidin-2-amine (3b) (46.0mmole). N, N dicyclohexylcarbodiimide (46.0mmole) was dissolved in dichloromethane. The solution was stirred for 24 h at room temperature. A syrupy resin obtained was dried under vacuum. The resin was dissolved in 15 mL of acetone. A white precipitate of dicyclohexylurea (DCU) appeared was discarded and filtrate was collected. The final filtrate was evaporated to

afford the product syrupy liquid, yield 85 %; density: 1.022cm<sup>3</sup>; IR (KBr)  $\lambda_{\max}/\text{cm}^{-1}$ : 3440 (-OH, -NH), 2915 (-CH<sub>2</sub>-PEG), 2895 (-CH<sub>3</sub>), 1715 and 1620 cm<sup>-1</sup> for the ester and amid bond (-C=O, PEG), 1525 (-NO<sub>2</sub>); <sup>1</sup>H NMR (400 MHz, CDCl<sub>3</sub>/DMSO-d<sub>6</sub>,  $\delta$ , ppm):  $\delta$  2.22 (s, 3H, -SCH<sub>3</sub>), 3.53-4.34 (m, multiple-H-PEG), 5.32 (s, 1H, -NH), 6.52 (s, 1H, Ar-H), 8.01-8.02 (d, 1H, *J*=4.36, Thiophene-H), 8.28-8.29 (d, 1H, *J* = 3.76, Thiophene-H); <sup>13</sup>C NMR (100 MHz, CDCl<sub>3</sub>/DMSO-d<sub>6</sub>,  $\delta$ , ppm):  $\delta$  13.93, 61.13-61.28, 64.10-64.26, 68.89, 69.96-70.31, 114.32, 118.65, 130.46, 143.23, 148.21, 149.16, 161.85, 162.51, 164.96, 165.41, 169.49; GCMS (m/z): 548 (M<sup>+</sup>), Molecular formula: PEG-C<sub>9</sub>H<sub>7</sub>N<sub>4</sub>O<sub>2</sub>S<sub>2</sub>.

#### Synthesis of PEGylated- 4-(furan-2-yl)-6-(methylthio)pyrimidin-2-amine (4c)

The mono acid derivative of carboxyhydroxy PEG (HO-PEG<sub>200</sub>COOH) (28.0mmole) was activated with 1:2 molar equivalent of 4-(furan-2-yl)-6-(methylthio)pyrimidin-2-amine (3c) (46.0mmole). N, N dicyclocarbidiimide (46.0mmole) was dissolved in dichloromethane. The solution was stirred for 24 h at room temperature. A syrupy resin obtained was dried under vacuum. The resin was dissolved in 15 mL of acetone. A white precipitate of dicyclohexylurea (DCU) appeared was discarded and filtrate was collected. The final filtrate was evaporated to afford the product syrupy liquid, yield 88 %; density: 1.260cm<sup>3</sup>; IR (KBr)  $\lambda_{\max}/\text{cm}^{-1}$ : 3320(-OH, -NH), 2925 (-CH<sub>2</sub>-PEG), 2850 (-SCH<sub>3</sub>), 1720 and 1625 cm<sup>-1</sup> for the ester and amid bond (-C=O, PEG); <sup>1</sup>H NMR (400 MHz, CDCl<sub>3</sub>/DMSO-d<sub>6</sub>,  $\delta$ , ppm):  $\delta$  2.09 (s, 3H, -SCH<sub>3</sub>), 3.51-4.27 (m, multiple-H-PEG), 4.81 (s, 1H, -NH), 6.07 (s, 1H, Ar-H), 6.47-6.48 (t, 1H, Furan-H), 7.19-7.25 (dd, 1H, *J*=3.48, 4.24 Furan -H), 7.42-7.48 (dd, 1H, *J* = 4.8, 3.44 Furan -H); <sup>13</sup>C NMR (100 MHz, CDCl<sub>3</sub>/DMSO-d<sub>6</sub>, ppm):  $\delta$  13.85, 60.29-72.34, 107.53, 111.89, 114.11, 141.96, 148.83, 156.85, 165.30, 166.50, 168.80, 169.00, 169.82; GCMS (m/z): 487 (M<sup>+</sup>), Molecular formula: PEG- C<sub>9</sub>H<sub>8</sub>N<sub>3</sub>SO.

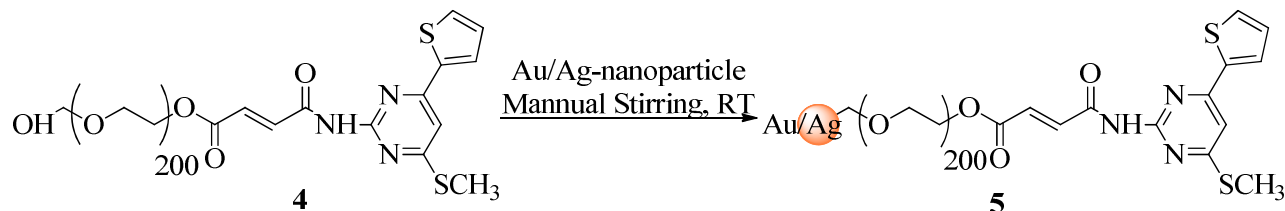
#### Preparation of colloidal gold and silver nanoparticles

Gold chloride (4%) solution and 1% sodium citrate solution were made in deionized H<sub>2</sub>O (DIH<sub>2</sub>O). One liter of the 4% gold chloride solution was under reflux during the addition of 80 mL of sodium citrate solution. The addition of sodium citrate solution to the gold chloride initiated a series of reduction reactions characterized by changes in the color of the initial gold chloride solution. After particle synthesis, the solution was cooled to room temperature; the gold nanoparticles were concentrated by centrifugation of the reaction mixture at 16000 rpm for 30min at room temperature, and then were collected for further characterization.

In a 1L flask, a solution of 90 mg AgNO<sub>3</sub> in 500mL of triply distilled H<sub>2</sub>O was brought to boiling with rapid stirring. To this solution was added 10mL of 1% sodium citrate. The reaction mixture was boiled for 30min, and then it was diluted up to 420mL. A series of reduction reactions were characterized by changes in the color. The AgNPs were concentrated by centrifugation of the reaction mixture at 10,000 rpm for 10min twice, and then were collected. All nanoparticles were stored at room temperature in dark bottles and were generally used within 1-2 months after preparation.

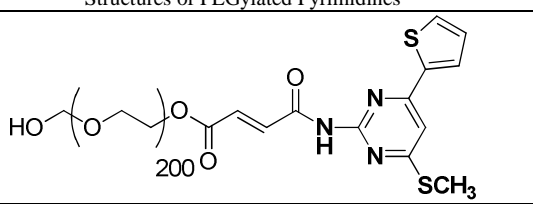
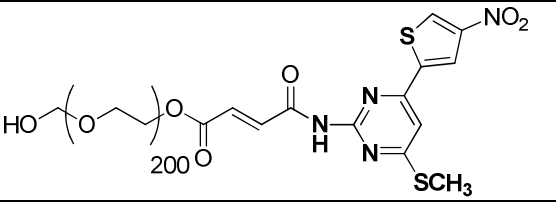
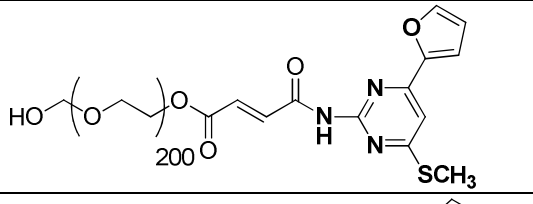
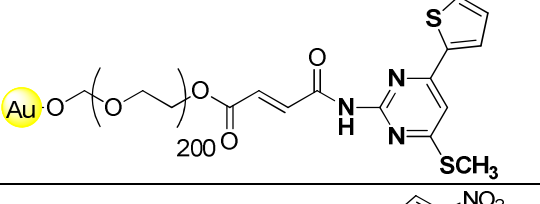
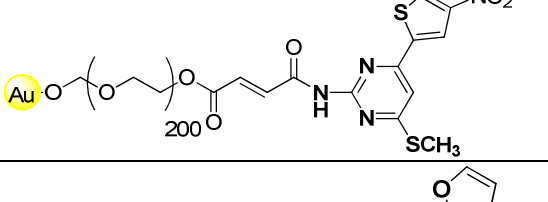
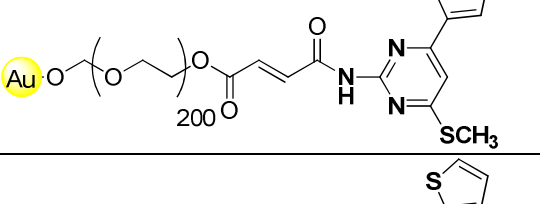
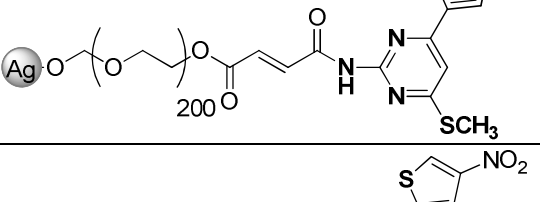
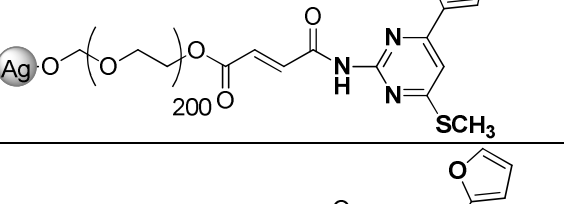
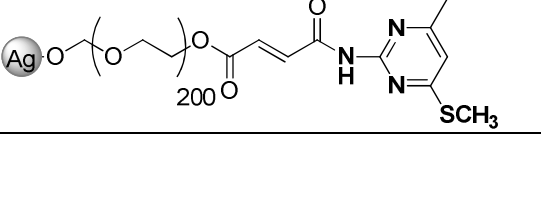
#### Surface functionalization of gold/silver nanoparticles with pegylated pyrimidine (5a-f)

PEGylated-pyrimidine prepared as described in the preceding section was added to the aqueous dispersion of gold/silver nanoparticles and the reaction was carried out for conjugation of the fluorescence dye to the gold surface through the alcoholic functionality at room temperature (Table 2, Scheme 5). Fluorescent conjugated nanoparticles were separated from free pyrimidine PEG hydroxyl group by centrifugation with several washings. Attachment of PEGylated pyrimidine onto the surface of gold/silver nanoparticles was confirmed by the fluorescence that was observed by UV-Visible spectrophotometer.



Scheme 5 Synthesis of PEGylated-pyrimidines and surface passivation onto gold and silver nanoparticles 5

Table 2 Structures of PEGylated pyrimidines surfacted onto Au/Ag NPs

S. No.	Structures of PEGylated Pyrimidines	Density (d) in $\text{cm}^3$
4a		1.154
4b		1.022
4c		1.126
5a		1.134
5b		1.134
5c		1.108
5d		1.11
5e		1.086
5f		1.102

## Biology

### Antioxidant activity

#### DPPH assay method

Free radical scavenging activity of the test compounds **4** and **5** was determined by the 1,1-diphenyl picrylhydrazyl (DPPH) assay method [18]. Drug stock solution (1 mg mL<sup>-1</sup>) was diluted to final concentrations of 2, 4, 6, 8 and 10 mg mL<sup>-1</sup> in methanol. DPPH methanol solution (1 mL, 0.3 mmol) was added to 2.5 mL drug solutions of different concentrations and allowed to react at room temperature, 30 min later; the absorbance was measured at 518 nm. Lowered absorbance of the reaction mixture indicated higher free radical scavenging activity and was calculated as per the following equation.

$$\text{DPPH Scavenging effect} = \left[ \frac{(\text{Abs control} - \text{Abs blank}) \times 100}{\text{Abs control}} \right]$$

### Anti-proliferative activity

#### Assay principle:

In this assay the viability of chemically treated cells are measured by a dye, Resazurin or Alamar blue (AB). AB, a non-fluorescent indicator dye, is converted to bright red-fluorescent resorufin via the reduction reactions of metabolically active cells. The amount of fluorescence produced is directly proportional to the number of living cells.

*Protocol:* Standard Alamar blue assay protocol for cell viability assay was used. U2OS human osteosarcoma cells were grown in RPMI-1640 medium, MB231 human breast cancer cell line were grown in DMEM medium, and SW480 cells were grown in Leibovitz's L-15 medium. All the cell culture media were supplemented with 10% FBS, 0.1% nonessential amino acids, 100 µM/mL penicillin, and 100 unit/mL streptomycin. The cells were separately seeded into 96-well plates at the density of 1x10<sup>4</sup> cells/well and incubated at 37 °C, 5% CO<sub>2</sub> for 24 hours before experiment. Next day, the medium was replaced with medium containing appropriate concentration of the compounds. Test compounds were diluted with corresponding culture media to different concentrations. Pure drug, doxorubicin was used as control. The maximum concentration of each compound was 4000 µg/mL. 1/6 dilution was used for each compound. The cells were treated for 48 h and 2 µL of Alamar blue was added to each well and incubated for two hours. Fluorescence intensity was read with plate reader the percentage growth inhibition was observed. IC<sub>50</sub> value was calculated from the graph. The effect of all new compounds on various cancer cell lines U2OS, MB231 and SW480 was observed and results are reported. Growth inhibition % was compared with standard drug doxorubicin. For rows, alcohol was added to generate killed cells.

## RESULTS AND DISCUSSION

### Chemistry

The focal point of our research was to determine effective synthetic routes for the preparation of novel pyrimidine hybrids. We have developed facile methods to prepare high value pyrimidine derivatives adorned with thiophene and furan ring within the same molecular framework. Another convenient methodology has been efficiently employed to afford their nitro derivative.

The synthesis of 4-(methylthio)-6-(thiophen-2-yl) pyrimidin-2-amine **3** was accomplished starting with 2-acetyl thiophene **1**. NaH in dry toluene at 0°C was added to 2-acetyl thiophene **1** with constant stirring for 10 min. Carbon disulphide and methyl iodide were added to the cold solution and the reaction mixture was kept for 24 h under stirring condition furnished 3,3-bis(methylthio)-1-(thiophen-2-yl)prop-2-en-1-one **2**. However, reaction of **2** with guanidine carbonate and NaH in dry DMF afforded 4-(methylthio)-6-(thiophen-2-yl) pyrimidin-2-amine **3** under reflux for 6 h.

The PEGylation chemistry has been successfully demonstrated at the amino group situated at C-2 of pyrimidine hybrids (Scheme 5). To couple a PEG to a pyrimidine molecule, it is first necessary to 'activate' the polymer by converting the hydroxyl terminus to some functional group capable of reacting with the functional group situated on pyrimidine molecule. We opted to activate the PEG by converting it to its acid derivative and coupling it with amino group of pyrimidine molecule. This PEGylation methodology involves conjugation of pyrimidine onto hetero bi-functional PEG derivatives having -OH on one terminus and -COOH on the other for covalent attachment of amino group. The free carboxyl group was used for conjugation via amine coupling. We have determined that this conjugation proceeds through formation of amide linkage between the PEG chain and pyrimidines under mild reaction conditions.

“Small is beautiful”: today we know that small is not only beautiful but also smart and powerful. This is our one of the major concerns in synthesis of gold and silver nanoparticles with specific core, size and morphology. We have



advanced our earlier work on in-vitro anticancer evaluation of PEGylated quinolones against diverse cancer cell lines such as HCT116, H1299, COLO 205, MDA-MB 231, MDA-MB 468, SW 480 and SW 620. The results prompted us to investigate PEGylated pyrimidines and their gold and silver nano-particle conjugated derivatives against diverse cancer cell lines.

The nanoparticles of gold were prepared by reduction of gold hypochlorite with freshly prepared tri-sodium citrate whereas silver nano particles were prepared by boiling  $\text{AgNO}_3$  solution with sodium citrate buffer. The formation of Au/Ag nanoparticles was confirmed by change in color of reaction mixture and UV-visible spectroscopic analysis. The size of nanoparticles has been confirmed by TEM, showed the formation of spherical 20 nm sized particles. All nano particles were stored at room temperature in dark bottles and were generally used within 1-2 months after preparation.

The surface passivation means adding biomolecule functionality onto the surface of metal nanoparticles to improve the specificity and internalization of nanoparticles in various biomedical applications. To increase the targeting potential and circulation time, we have incorporated the surface passivation of nanoparticles. Pyrimidine hybrids, pharmacophores linked with the polyfunctional PEGylated polymer have been successfully attached to nanoparticles. Initially, PEGylated pyrimidines displayed a green fluorescence. The progress of surface passivation on to nanoparticle was confirmed by gradual decrease of fluorescence quenching effect.

We have prepared novel PEGylated pyrimidine derivatives possessing favorable reaction kinetic in both the Staudinger and Mitsunobu etherification reactions. Furthermore, the synthesized compounds **4** and **5** were evaluated for their antioxidant activity, *in-vitro* anti-cancer.

The chemical structures of the target compounds were confirmed by IR,  $^1\text{H}$ NMR,  $^{13}\text{C}$ NMR, MASS, CHN analysis, TEM, XRD and UV spectroscopy.

Contributing to the elucidation of the structures of compounds **3a-c** (Table 1), the infrared spectra showed two peaks at  $3400\text{-}3200\text{cm}^{-1}$  corresponding to  $-\text{NH}_2$  group, peaks at  $2920\text{-}2915\text{cm}^{-1}$  owing to  $-\text{CH}_3$ , peaks at  $1610\text{-}1590$  described  $-\text{C}=\text{C}-$  stretching in aromatic ring. IR spectra of compound **4a-c** exhibited intense broad peaks at  $3395\text{-}3320\text{cm}^{-1}$  accounted for  $-\text{OH}$  and  $-\text{NH}$  group. The peaks at  $2925\text{-}2915\text{cm}^{-1}$  appeared due to  $-\text{CH}_2\text{-PEG}$ . The characteristic bands associated with esters and ethers of PEG linker appeared at  $1720$  and  $1625\text{cm}^{-1}$  respectively.

$^1\text{H}$ NMR ( $\text{CDCl}_3/\text{DMSO}_d_6$ ) was nicely resolved for compounds **3a-c** and showed singlets in the range of  $\delta$  2.45-2.64 resonating for  $-\text{SCH}_3$  protons, appearance of  $-\text{NH}_2$  protons as a characteristic singlet in the range of  $\delta$  4.80-5.04, aromatic protons of pyrimidine ring in the range of  $\delta$  6.36-6.76, supported the assigned structure. The signals appeared at  $\delta$  7.01-7.99 resolved aromatic protons of thiophene/furan attached to pyrimidine ring at C-6 in all **3a-c**. In  $^1\text{H}$ NMR spectra of compounds **4a-c**, disappearance of the signals  $\delta$  4.80-5.04 of  $-\text{NH}_2$  protons and the appearance of multiplets in the up field  $\delta$  3.22-4.55 for PEG polymer clearly indicated the formation of PEGylated pyrimidines. Additionally, the characteristics signals appeared at  $\delta$  4.81-5.67 confirmed the formation of new functionality -CONH by PEG polymer and pyrimidine linkages.  $^{13}\text{C}$ NMR spectra of **3a-c** also supported the assigned structures. The signals at  $\delta$  126-129 ppm indicated the presence of thiophene ring in **3a**. The  $^{13}\text{C}$ NMR spectra also supported the structures of **4** and **5**. Peaks in the range of  $\delta$  12.56-13.96 ppm related to the  $-\text{SCH}_3$  and signals in the range of  $\delta$  164-169 ppm indicated the presence of carbonyl carbon ( $-\text{C}=\text{O}$ ). Signals at  $\delta$  60.29-72.34 indicated the presence of PEG linker and  $-\text{CH}_2$  linkages appeared at downfield region due to ether linkages. The mass spectral data also lent credence to the assigned structures.

### Characterization of the colloidal gold and silver nanoparticles

#### UV-Visible Spectroscopy

Initially, the formation of gold/silver nanoparticles was visually confirmed by color change from colorless to yellowish for silver and ruby red for gold nanoparticles. The reaction was completed within 10 and 30min respectively. The preliminary investigation of formation of the gold and silver nanoparticles was carried out by UV-visible spectroscopic analysis. A medium peak of absorbance at higher wavelength 518nm was observed. The intensity of the peak was increased in 10 min which confirmed the formation of Au nano particles. There was no significant shift of absorption observed but the intensity of the peak was steadily increased as the function of time reaction. In case of silver nanoparticles, the absorption was observed at 400 nm, similarly the intensity of the peak was steadily increased as the function of time reaction. The formation of gold and silver nanoparticles was also supported by TEM analysis. The gold and silver nanoparticles were observed to be extremely stable in the solution even for eight weeks after their synthesis. The results were in accordance with the literature methods[19]. The plots of the absorbance at  $\lambda_{\text{max}}$  (nm) vs. time (min) of reaction were shown in the sets of Figure 2a and b and ratified the rapid formation of nanoparticles in this process. From the UV-visible spectra, it was found that the reduction of  $\text{Au}^{3+}$

and  $\text{Ag}^+$  ions were completed within 10-30 min respectively. The formation of gold nanoparticles was faster than the silver nanoparticle which was mostly likely due to the difference in the reduction potential of two metal ions.

The preliminary characterization of compound **4a** was done by UV-Visible, CHN, IR,  $^1\text{H}$ NMR,  $^{13}\text{C}$ NMR and MASS. The UV-visible analysis of compound **4a** showed the absorbance at 325nm (Figure 2c).

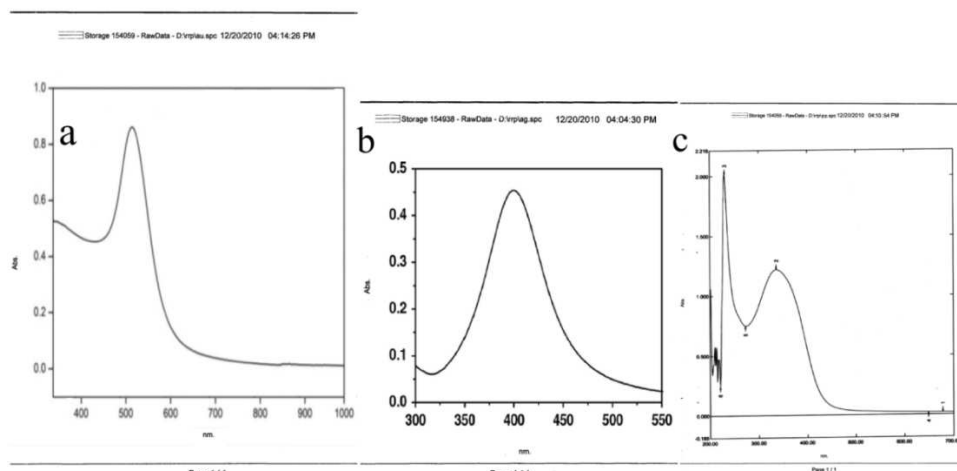


Fig. 2 UV-Vis spectrum of a) gold, b) silver nanoparticles and c) PEGylated-pyrimidine

We speculated that the PEGylated pyrimidines were linked with the nanoparticles the surface passivation was confirmed by UV-Visible analysis depicted in the Figure 3a and b for gold and silver nanoparticles respectively. The attachment of PEGylated pyrimidines onto the surface of gold/silver nanoparticles was confirmed by fluorescence observed in UV-visible spectrophotometer.

In the Figure 3a, a signal due to PEGylated pyrimidine was completely diminished. Moreover, no signal appeared at 518 nm for Au-nanoparticle. A new signal appeared at 528 nm showed a red shift which confirmed the formation of conjugated Au nanoparticles with PEGylated pyrimidines. The absorbance at 420 nm confirmed the formation of Ag-nanoparticle linked with PEGylated pyrimidine (Figure 3b). In both the cases, the absorbance recorded in the red shift region, supported surface passivation of the nanoparticles loaded with PEGylated pyrimidines.

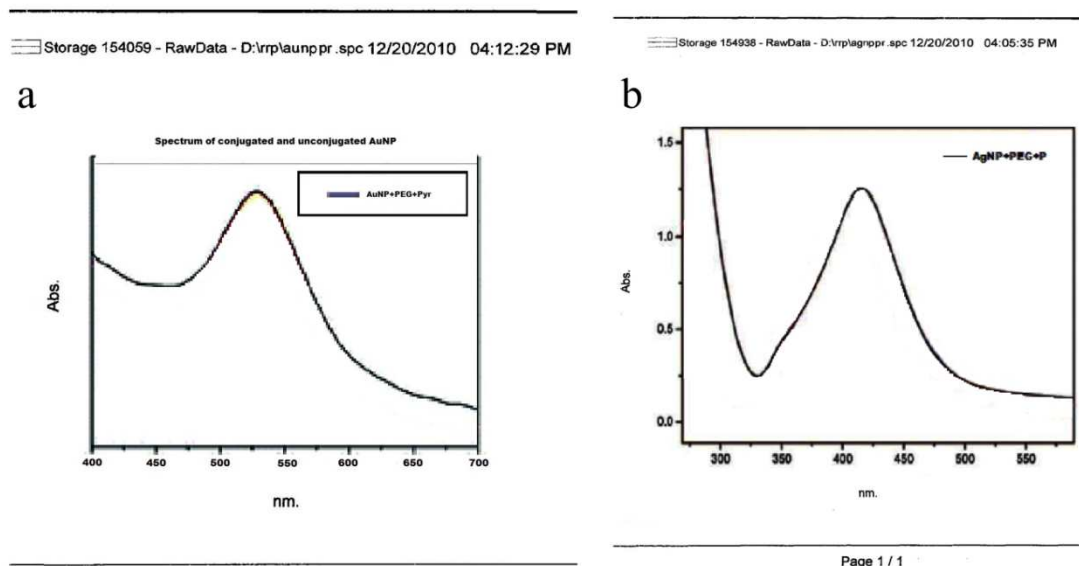


Fig. 3 UV-Vis Spectrum of a) gold and b) silver nanoparticles conjugated with PEGylated pyrimidine

#### Transmission electron microscopy analysis (TEM)

Direct evidence concerning the morphology and inter-particle spacing comes from transmission electron microscopy studies of colloidal gold/silver PEG solution on copper TEM grids. The TEM images of gold and silver nanoparticles are depicted in (Figure 4a and b) respectively. Gold nanoparticles synthesized by the reported method have a propensity of forming the spherical particles. In addition, from the images it was observed that the particles

formed with triangular and hexagonal shapes. The size of gold/silver nanoparticles was found in the range of 9 nm to 31 nm. The average size of the nanoparticle was found to be 12nm and 20nm respectively. The stability of the product is an important criterion in synthesizing nanoparticles. To stabilize the gold and silver nanoparticles, we employed PEG<sub>200</sub>. The Au/Ag nanoparticles were stable for two months, while those without stabilizer were stable for one week. The cluster formation was observed by agglomeration of two to many gold/silver nanoparticles. The examination of these images verifies the fact that the size of the nanoparticles are uniform and defined solely by particle diameter, the particles are closely spaced in the form of clusters and strings. The tendency of formation of aggregation of particles was observed in both the cases. In general, it is known that, by electrostatic factors, colloidal particles are negatively charged and thus naturally repel one another. But in both the cases, we observed the occurrence of aggregation however the inter-particle repulsion is predominated.

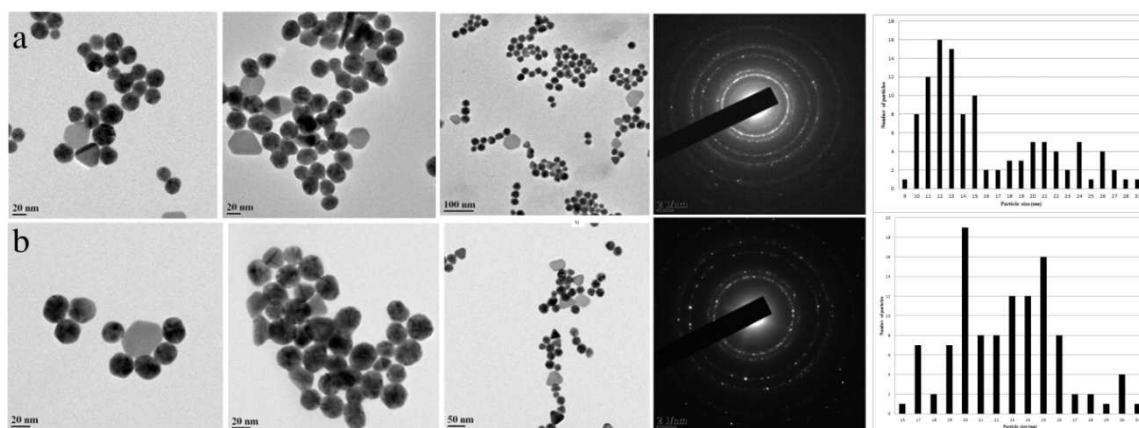


Fig. 4 TEM, SAED and size distribution histogram from TEM analysis (left to right) of a) gold and b) silver nanoparticles

The selected area electron diffraction patterns(SAED) and size distribution of gold and silver nanoparticles are shown in the Figure4a and b. Electron diffraction pattern confirmed the formation of crystalline gold and silver nanoparticle.

#### X-ray diffraction analysis (XRD)

The XRD pattern recorded for both gold and silver nanoparticles show four intense peaks in the whole spectrum of  $2\theta$  values ranging from 20 to 80. Figure5a and b shows the XRD patterns obtained for the silver and gold nanoparticles. The presence of intense peaks of nanoparticles (1 1 1), (2 0 0), (2 2 0) and (3 1 1) appeared which are indexed as crystalline gold and silver face centered cubic phase. The standard XRD patterns for Au and Ag are almost similar [Joint Committee on Powder Diffraction Standards (JCPDS) file no: 01-1174 for Au and 04-0783 for Ag]. The XRD pattern thus clearly shows that the gold and silver nanoparticles formed by the chemical reduction of  $\text{AuCl}_4^-$  and  $\text{Ag}^+$  ions are crystalline in nature.

The broadening of Bragg's peak indicated the formation of gold and silver nanoparticles. The mean size of gold and silver nanoparticles was also calculated using the Debye-Scherrer's equation by determining the width of the (1 1 1) Bragg's reflection. The mean size of gold and silver nanoparticles determined from XRD patterns are well in accordance with from the size analyzed from TEM images. In present case, the average diameter obtained from TEM and XRD analysis was 12nm and 20 nm for gold and silver nanoparticles respectively.

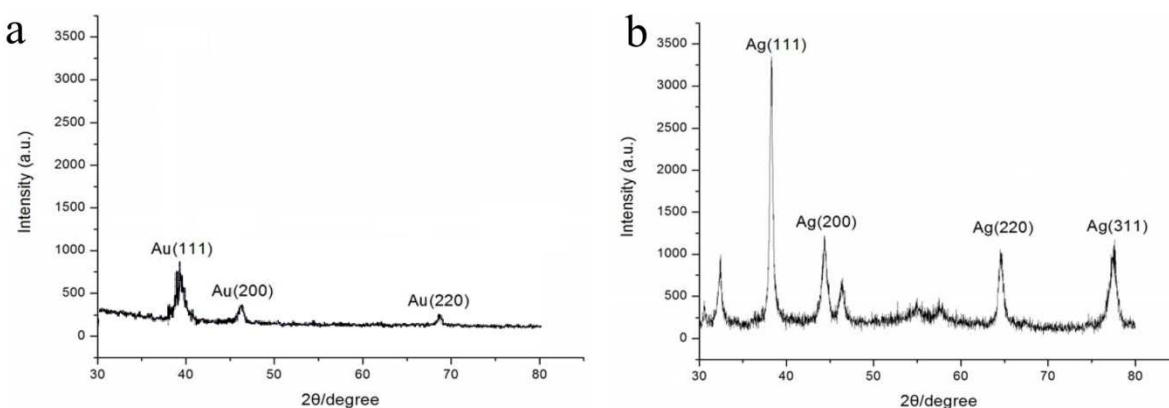


Fig. 5 XRD patterns of (a) gold and (b) silver nanoparticles

We observed the formation of gold and silver particles uniformly. In surface passivation we presume that once the nuclei after reaction with Au and Ag ions get formed, adsorption of –OH takes place on the surface. In this step which might serve as the rate determining for the growth of the particles in Figure 6a-b and displayed a significant role.

Also the possibility of adsorption at specific planes cannot be ruled out thus facilitating the growth of specific shape of the particles in Figure 6a-b. The diffused density has been observed suggested the surface passivation of PEGylated aminopyrimidines on to gold and silver nanoparticles.

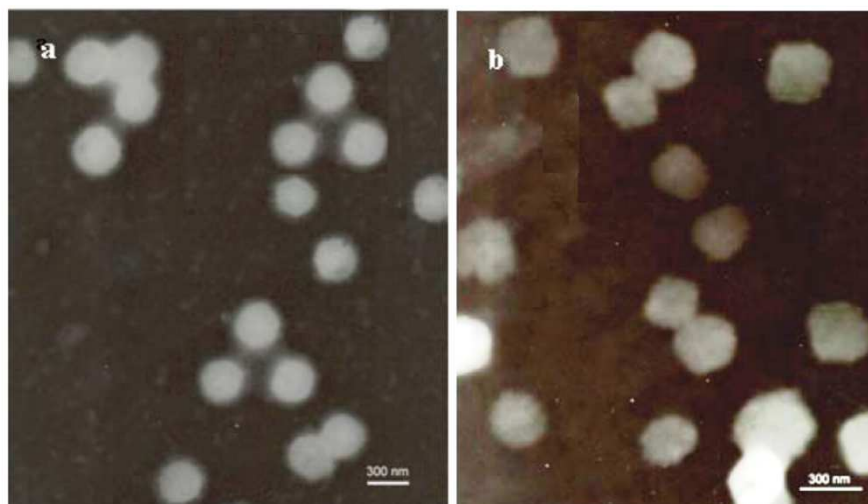


Fig. 6 TEM image of a) gold and b) silver nanoparticles conjugated with PEGylated pyrimidine

#### Antioxidant activity

Free radical scavenging activity of the test compounds **4** and **5** was determined by the 1,1-diphenyl picrylhydrazyl (DPPH) assay method[18]. Drug stock solution ( $1 \text{ mg mL}^{-1}$ ) was diluted to final concentrations of 20, 40, 60, 80 and  $100 \mu\text{g mL}^{-1}$  in methanol. DPPH methanol solution (1 mL, 0.3 mmol) was added to 2.5 mL drug solutions of different concentrations and allowed to react at room temperature. After 30 min the absorbance values were measured at 518 nm and converted into the percentage antioxidant activity. Methanol was used as the solvent and ascorbic acid as the standard. The percentage of inhibition extrapolated against concentration is depicted in Figure 7. Results are presented in Table 3. The standard drug used was ascorbic acid. The DPPH scavenging effect is given by the formula:

$$\text{DPPH Scavenging effect} = \left[ \frac{(\text{Abs control} - \text{Abs blank}) \times 100}{\text{Abs control}} \right]$$

Table 3 Antioxidant activity of the compounds **4** and **5**

Compound Code	20 $\mu\text{g/ml}$	40 $\mu\text{g/ml}$	60 $\mu\text{g/ml}$	80 $\mu\text{g/ml}$	100 $\mu\text{g/ml}$
<b>4a</b>	14	17	20	22	25
<b>4b</b>	14	16	16	22	28
<b>4c</b>	6	6	8	9	10
<b>5a</b>	16	21	25	28	32
<b>5b</b>	12	18	20	24	28
<b>5c</b>	5	7	8	8	9
<b>5d</b>	14	14	18	23	30
<b>5e</b>	13	16	22	24	26
<b>5f</b>	5	6	7	9	10
Ascorbic acid	10	15	20	33	56

From Table 3 it was found that **5a** and **5d** displayed excellent antioxidant activity at all concentrations. The rest of the compounds **4a**, **4b**, **5b** and **5e** also showed considerable antioxidant activity. The thiophene ring at pyrimidine nucleus connected to linker PEG with Ag and Au nanoparticles may be accountable for momentous antioxidant activity. The decline in antioxidant activity of compounds **4c**, **5c** and **5f** suggested discarding the molecules for further investigation of anti-cancer activity.

The significant antioxidant activities of compounds **4** and **5** prompted us to investigate anti-proliferative activities of all these compounds.

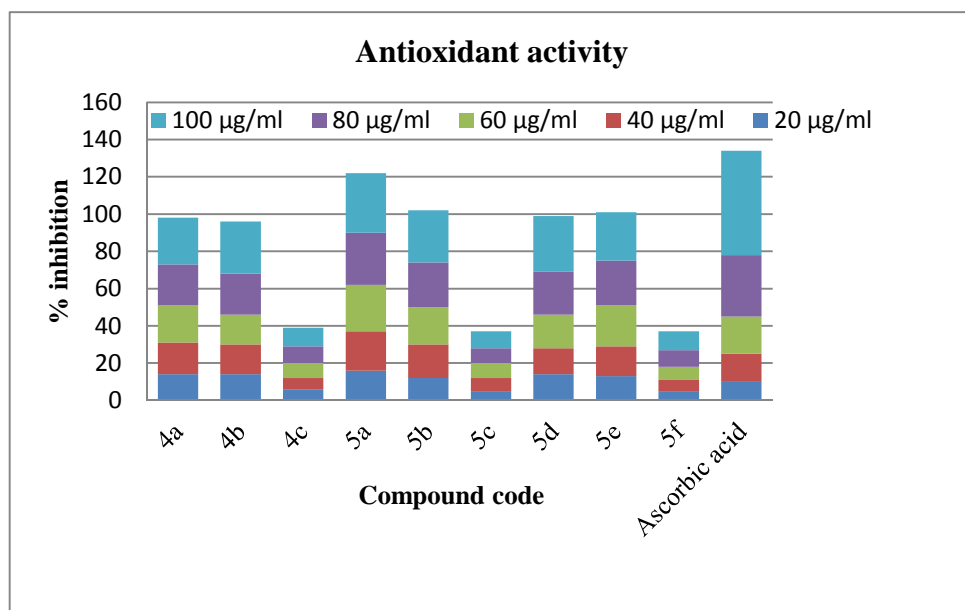


Fig. 7 Antioxidant activity of compounds **4** and **5**

### Pharmacology

#### Anti-proliferative activity

The exact mechanism by which the gold and silver nanoparticle conjugated with biomolecule inducing anticancer activity is unclear but it is known that they are directly cytotoxic and many appear to have anti-mitochondrial activity as well as the formation of DNA strands breaks and DNA proteins cross links[20-23].

In the Alamar blue assay, the percentage of reduction of cancer cells is time dependent, thus, more percentage of reduction suggested the more proliferative activity of the cancer cells. The cell viability of U2OS human osteosarcoma cell line, MB231 human breast cancer cell line and SW480 colon carcinoma cell line was investigated at various concentrations of the tested compounds. All eight compounds were tested in Alamar blue assay (in the case of leukemia cells) for their anti-proliferative activity *in vitro* against three human cancer cell lines, U2OS osteosarcoma cell line, MB231 breast cancer cell line and SW480 colon carcinoma obtained from ATCC. Two sets of experimentations have been carried out at various concentrations to acquire the authenticity of the obtained results in percentage growth inhibition. From these observations, the percentage mean growth inhibition was calculated and the graphs were plotted as mean percentage growth inhibition. Doxorubicin (250 µM) was applied as a referential cytotoxic agent (positive test control). The results of cytotoxic activity *in vitro* were expressed as an  $ID_{50}$  (µM/mL), i.e., the concentration of compound, which inhibits the proliferation of 50% of tumor cells as compared to the control untreated cells. A value of less than 10µM/mL was considered as an anti-proliferative activity criterion for synthetic compounds.

The cytotoxicity results of tested compounds in U2OS and doxorubicin are depicted in Table 4 (Figure8). The relative study of concentrations of synthesized compounds and doxorubicin was compared; it was observed that at 4000µM the compounds showed the highest inhibition, whereas doxorubicin showed highest inhibition at 333µM. These outcomes suggested that the efficacy of the test compounds is 12 folds lesser than doxorubicin. The  $IC_{50}$  values are illustrated in Table 4. The  $IC_{50}$  values of compounds **4a**, **4b**, **5b**, **5d**, were 13 µM, 26 µM, 16 µM, 33 µM respectively. Compounds **3a**, **3b** and **5a** possessed highest  $IC_{50}$  values i.e., in the range 181 to 526µM. Compound **5e** possessed  $IC_{50}$  value 81. These  $IC_{50}$  values suggested that compounds **4a**, **4b**, **5b** and **5d** have highest anticancer activity. Compound **5e** has good activity while the rest of the compounds possess moderate anticancer activity.

Table 4 % Growth inhibition in U2O Sosteosarcoma cell line

Sr. No	Conc.	3a	3b	4a	4b	5a	5b	5d	5e	Conc.	Doxo.
1	4000	102	105	93	102	102	102	102	102	333	101
2	667	72	53	104	100	100	75	104	102	56	103
3	111	47	41	83	63	39	19	58	27	9	100
4	19	46	48	56	49	40	51	48	44	2	84
5	3	36	43	38	35	26	43	34	40	0.3	57
6	1	34	46	45	31	25	31	29	41	0.04	38
7	0	27	41	31	19	17	24	23	32	0.01	8
8	IC <sub>50</sub>	181	526	13	26	213	16	33	81	0.18	

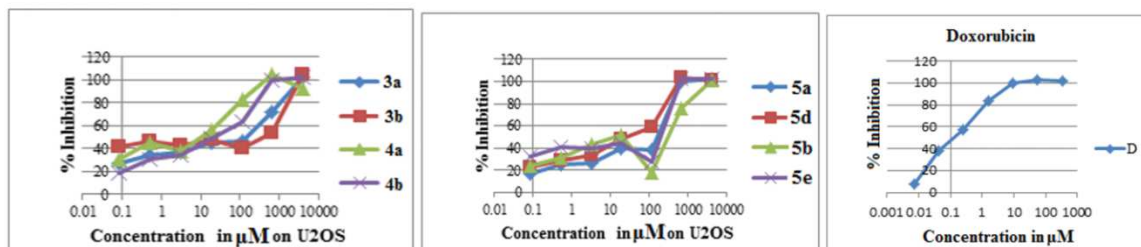


Fig. 8 Anti-proliferative activity of compounds 3a, b - 4a, b, 5a, d, b, e and doxorubicin against: U2OS cancer cell line

The percentage growth inhibition of MB231 and SW480 cancer cell lines are exemplified in Tables 5 and 6 at various concentrations and results are compared with doxorubicin. The IC<sub>50</sub> values ranging from 137 to 530 μM indicated that the compounds exhibited moderate potency in MB231 (Table 5, Figure 9). However, compounds **4a** and **4b** having IC<sub>50</sub> values 19 & 46 μM respectively, anticipated the highest anticancer activity against MB231 human breast cancer cell.

Table 5 % Growth inhibition in MB231 breast cancer cell line

Sr. No	Conc.	3a	3b	4a	4b	5a	5b	5d	5e	Conc.	Doxo.
1	4000	101	101	98	101	101	101	100	101	333	100
2	667	56	54	100	101	102	102	102	100	56	100
3	111	34	36	79	70	33	44	47	43	9	99
4	19	34	39	38	41	26	40	33	40	2	89
5	3	33	41	45	48	37	44	39	43	0.3	75
6	1	31	38	45	34	34	35	31	40	0.04	55
7	0	30	22	31	24	63	35	29	37	0.01	41
8	IC <sub>50</sub>	512	530	19	46	247	168	137	181	0.03	

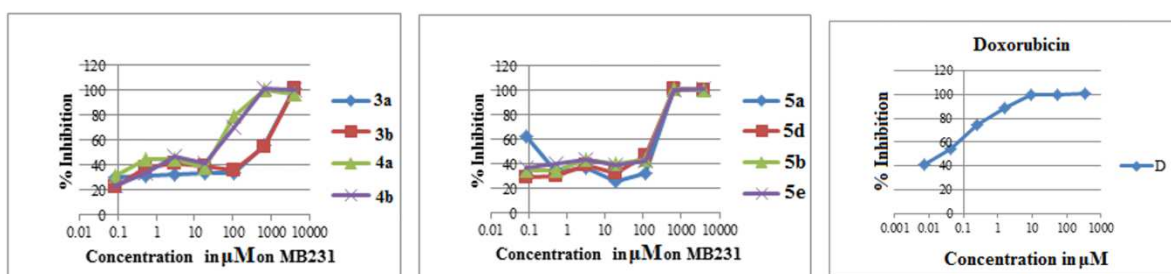


Fig. 9 Anti-proliferative activity of compounds 3a, b - 4a, b, 5a, d, b, e and doxorubicin against: MB231 cancer cell line

Table 6 % Growth inhibition in SW480 colon cancer cell line

Sr. No	Conc.	3a	3b	4a	4b	5a	5b	5d	5e	Conc.	Doxo.
1	4000	101	99	99	101	101	101	100	101	333	98
2	667	17	13	100	100	98	90	100	96	56	95
3	111	0	10	27	14	15	16	14	7	9	97
4	19	6	10	3	13	17	24	14	12	2	74
5	3	13	6	12	12	21	31	18	29	0.3	66
6	1	10	5	11	13	21	16	20	20	0.04	44
7	0	14	7	8	13	18	9	10	13	0.01	37
8	IC <sub>50</sub>	1702	6090	287	294	346	215	289	213	0.1	

In addition, all the compounds displayed moderated anticancer activity against the SW480 at IC<sub>50</sub> concentration in the range from 213 to 609 $\mu$ M. Comparatively, **4a**, **4b**, **5b**, **5d** and **5e** exhibited significant potency against all the said cancer cell line and the rest of the compounds displayed moderate activity (Table 6, Figure 10).

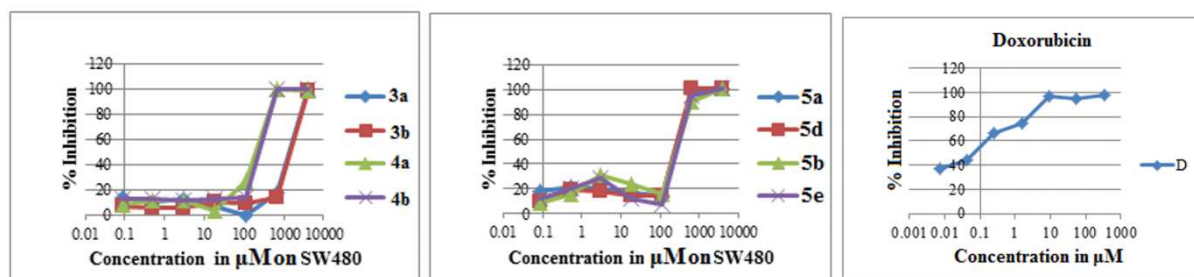


Fig. 10 Anti proliferative activity of compounds 3a, b -4a, b,5a, d, b, e and doxorubicin against: SW480 cancer cell line

The results summarized in the Table 7 (Figure 11), suggested that the compound **4a** proved to be a highly potent candidate against U2OS and MB231. These findings suggested that all the compounds exhibited significant to moderate anti-proliferative activity against U2OS human osteosarcoma, MB231 human breast cancer and SW480 colon carcinoma cell lines. When we compared the IC<sub>50</sub> values of all the compounds, this implies that after PEGylation, these anti-cancer activities were enormously increased in multiples of 0.85 to 32.9 folds.

Table 7 Relative efficacy of compounds 3-5

Sr No.	U2OS (Osteosarcoma cell line)			MB231(Breast cancer cell line)			SW480 (Colon cancer cell)		
	Before Pegylation	After Pegylation	Improvement in efficacy (Fold)	Before Pegylation	After Pegylation	Improvement in efficacy (Fold)	Before Pegylation	After Pegylation	Improvement in efficacy (Fold)
	IC <sub>50</sub> values in $\mu$ M	IC <sub>50</sub> values in $\mu$ M		IC <sub>50</sub> values in $\mu$ M	IC <sub>50</sub> values in $\mu$ M		IC <sub>50</sub> values in $\mu$ M	IC <sub>50</sub> values in $\mu$ M	
1	181	(3a) 13	13.9	512	(3a) 19	26.9	1702	(3a) 287	5.9
2	181	(3a) 213	0.85	512	(3a) 247	2.1	1702	(3a) 346	4.9
3	181	(3a) 33	5.9	512	(3a) 137	3.7	1702	(3a) 289	5.9
4	526	(3b) 26	20.2	530	(3b) 46	11.5	6090	(3b) 294	20.7
5	526	(3b) 16	32.9	530	(3b) 168	3.1	6090	(3b) 215	28.3
6	526	(3b) 81	6.5	530	(3b) 181	2.9	6090	(3b) 213	28.6
Doxorubicin=250 $\mu$ M			0.18	0.03			0.1		

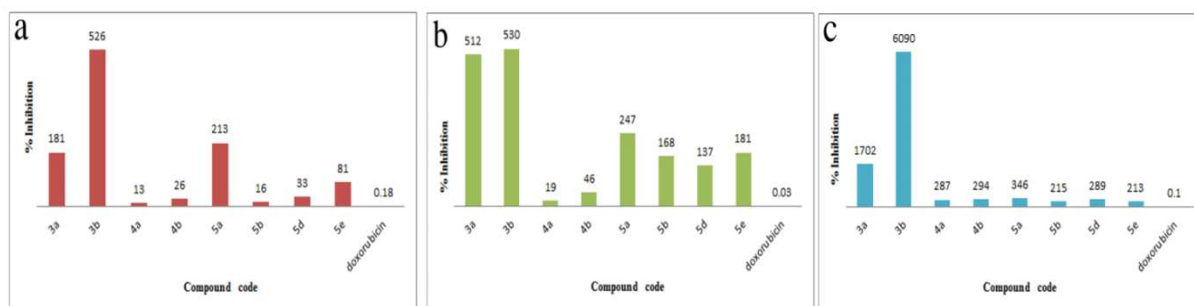


Fig. 11 Anti-proliferative activity of synthesized compounds against: a) U2OS b) MB231 and c) SW480 Cancer cell line

### Structure Activity Relationship

Depending upon the structural features, the newly synthesized molecules **4** and **5** could be divided into three discrete segments viz. diversely substituted central core pyrimidine ring A, nanoparticle (Au/Ag) surfaced with PEG as zone B and thiophene or furan ring C (X=S or O) (Figure12).

From Table 3 it was found that **5a** and **5d** displayed excellent antioxidant activity at all concentrations. The rest of the compounds **4a**, **4b**-**5e** also showed considerable antioxidant activity. The thiophene ring at pyrimidine nucleus connected to linker PEG with Ag and Au nanoparticles may be accountable for momentous antioxidant activity. The decline in antioxidant activity of compounds **4c**, **5c** and **5f** suggested discarding the molecules for further evaluation of anti-cancer activity. The significant antioxidant activities of compounds **4a-b** and **5a-b, d-e** prompted us to investigate anti-proliferative activities of all these compounds.

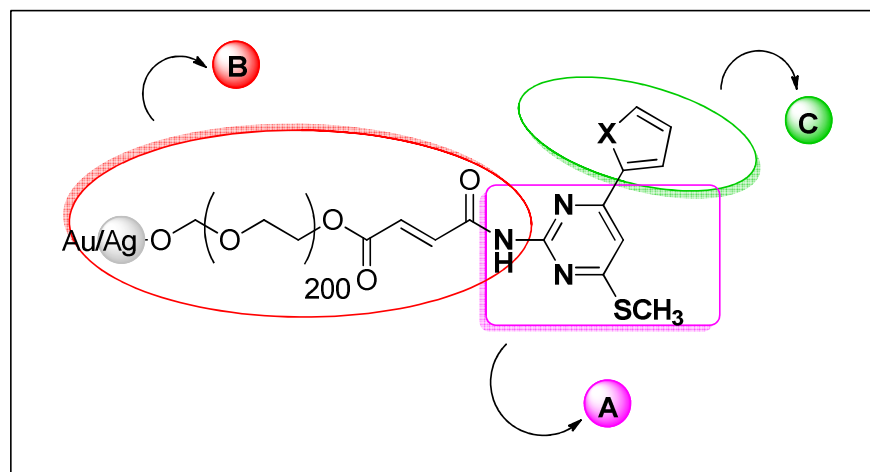


Fig. 12 Structure activity relationship of 4 and 5

The exceptionally high anticancer activity of PEGylated pyrimidine derivatives is suggestive of the fact that the enhanced efficacy of molecules may be because of the high mobility of the end terminal of the tethered PEG molecules and due to the presence of inter-repulsive forces exerted between the hydrated PEG chains, there is a strong possibility of single PEG molecule conjugation with the approaching protein.

### CONCLUSION

In conclusion, a new class of surface functionalized PEGylated-4-(methylthio)-6-(4-nitro/thiophene/furan-2-yl) pyrimidin-2-amines were synthesized. These compounds were used for surface activation on to synthesized gold/silver nanoparticles. Target analogs **4** and **5** were tested for anti-oxidant activity; the results exhibited that the PEGylated amino pyrimidines with thiophene ring at C2 position and its nitro derivative displayed significant anti-oxidant activity compared to that of its furan counterpart. As the compounds **4** and **5** exhibited momentous anti-oxidant activity, we proceeded to explore them as anti-cancer agents.

In this study, two independent approaches that conjugating pyrimidines to PEG<sub>(200)</sub> and mounting this passive targeting moieties onto the NPs were adopted to fabricate pyrimidine-PEG-AuNPs and pyrimidine-PEG-AgNPs. The NPs synthesized in this study were proven able to effectively target PEGylation to cancer cells, and showed profound apoptotic induction effect to those cells. Although the drug efficacy was compromised after conjugation with Au and Ag, the resultant could still make this moiety NPs a good candidate for anticancer therapy.

Our results supported the hypothesis that the nanoparticulated combinatorial drug delivery system for anticancer activities could improve the therapeutic outcome. The nanoparticle formulations described in this work were all simple, robust and easy to be fabricated. The materials chosen for the formulations were all bio-friendly, with minimum potential toxicity. Despite the positive and encouraging results with these nano particulate delivery systems observed in these studies, many further investigations remain to be done in the future, such as the genetic analysis of the therapeutic efficacy or alternative combination cocktail for other drugs or diseases.

### Acknowledgements

NKL express sincere gratitude to Dr. Mukund S. Chorghade, Dr. Manivasakam D. Palaniyandi and Ms. Tejashree Aurangabadkar for carrying out anti-cancer activity of synthesized compounds, Central instrumentation facility, Institute of Science, Nagpur for providing us Ultra Violet - Visible spectra, Department of Pharmacy, RTM Nagpur University for IR analysis, SAIF Chandigarh for <sup>1</sup>H NMR, <sup>13</sup>C NMR, and MASS analysis, SAIF IIT Mumbai for TEM analysis, SAIF IIT Chennai for elemental analysis. Special Thanks to UGC (UGC Major Project: 37-497/2009 [SR]), New Delhi for financial assistance.

### REFERENCES

- [1] Z Wang. Drug Delivery Systems for Antiangiogenesis and Anticancer Activities Ph.D. thesis, Department of Pharmacy, Nation University of Singapore, Singapore, **2010**.
- [2] NB Pathan; AM Rahatgaonkar; MS Chorghade. *Catalysis Communications*, **2011**, 12, 1170–1176.
- [3] Z Wufu; C Chen; S Chengyu; X Shan; W Chunjiang; L Fei; X Hui; T Qidong; Z Pengwu. *European Journal of Medicinal Chemistry*, **2015**, 93, 64-73.



- [4] KS Thriveni; B Padmashali; MB Siddesh; C Sandeep. *Indian J Pharm Sci*, **2014**, 76(4), 332-338.
- [5] CH Park; C Lee; JS Yang; BY Joe; K Chun; H Kim; HY Kim; JS Kang; JI Lee; MH Kim; G Han. *Bioorganic & Medicinal Chemistry Letters*, **2014**, 24, 2655–2660.
- [6] JS Yang; CH Park; C Lee; H Kim; C Oh; Y Choi; JS Kang; J Yun; JH Jeong; MH Kim; G Han. *European Journal of Medicinal Chemistry*, **2014**, 85, 399-407.
- [7] SB Katiyar; I Bansal; JK Saxena; PMS Chauhan. *Bioorganic & Medicinal Chemistry Letters*, **2005**, 15, 47–50.
- [8] X Tu, L Wang, Y Cao, Y Ma, H Shen, M Zhang, Z Zhang, *Carbon*, **2016**, 97, 35-44.
- [9] SA Chechetka; M Zhang; M Yudasaka; E Miyako. *Carbon*, **2016**, 97, 45–53.
- [10] NS Koseva; J Rydz; EV Stoyanova; VA Mitova. Hybrid Protein–Synthetic Polymer Nanoparticles for Drug Delivery: Advances in Protein Chemistry and Structural Biology. Academic Press, Rossen Donev, **2015**, 93-119.
- [11] PR Chandran; RT Thomas. Gold Nanoparticles in Cancer Drug Delivery: Nanotechnology Applications for Tissue Engineering. William Andrew Applied Science Publisher, **2015**, 221–237.
- [12] Z Wang; WK Chui; PC Ho. *Pharmaceutical Research*, **2009**, 26, 1162-1171.
- [13] VB Damodaran. Solid-phase protein PEGylation: Achieving mono-PEGylation through molecular tethering Ph.D. thesis, Chemical and Process Engineering, University of Canterbury, Christchurch, NZ, **2009**.
- [14] T Bruckdorfer. Drug delivery with PEGylation, *European Biopharmaceutical Review* (Spring): **2008**, 96-104.
- [15] Azaroff; Buerger. 'The powder method' McGraw Hill Book Co., Inc., New York, N. Y. **1958**.
- [16] WH Bragg; WL Bragg. 'The powder method' Bell, London, **1953**.
- [17] CW Bunn. 'Chemical Crystallography', Oxford University Press, Oxford, **1945**.
- [18] LL Mensor; FS Menzes; GG Leitao, et. al. *Phytother Res.*, **2001**, 15, 127-130.
- [19] RR Naik; SJ Stringer; G Agarwal; SE Jones; MO Stone. *Nat. Mater*, **2002**, 3, 1669-172.
- [20] SJ Berners-Prince; CK Mirabelli; RK Johnson; MR Matter; FL McCabe; LF Faucette; C Sung; S Mong; PJ Sadler; ST Crooke. *Cancer Research*, **1986**, 46, 5486-5493.
- [21] CK Mirabelli; RK Johnson; DT Hill; LF Faucette; GR Girard; GY Kuo; CM Sung; ST Crooke. *J Med Chem.*, **1986**, 29(2), 218-223.
- [22] GF Rush; PF Smith; DW Alberts; CK Mirabelli; RMSnyder; ST Crooke; J Sowinski; HB Jones; PJ Bugelski. *Toxicology and Applied Pharmacology*, **1987**, 90(3), 377-390.
- [23] PF Smith; GD Hoke; DW Alberts; PJ Bugelski; S Lupo; CK Mirabelli; GFRush. *J. Pharmacol. Exp. Therap.*, **1989**; 249(3), 944-950.